FULL PAPER

A Multifunctional Nanodevice Capable of Imaging, Magnetically Controlling, and In Situ Monitoring Drug Release

By *Shang-Hsiu Hu, Kuan-Ting Kuo, Wei-Lin Tung, Dean-Mo Liu,** and *San-Yuan Chen**

The multifunctional nanodevice described here integrates nanoscaled imaging, targeting, and controlled drug delivery, as well as the capability to monitor, in situ, the amount of drug released from the nanodevice with single-cell resolution. The nanodevice is composed of a polymer core/single-crystal iron oxide shell nanostructure bonded to a quantum dot. It shows outstanding release and retention characteristics via an external on/off manipulation of a high-frequency magnetic field. Upon magnetic stimulation, the single-crystal iron oxide shell demonstrates formation of nanometer-sized polycrystal domains of varying orientation. This allows a variation between retention and slow release of the drug. Further stimulation causes permanent rupturing of the shell, causing release of the drug in a burst-like manner. The quantum dot bonded to the nanodevice provides optical information for in situ monitoring of the drug release through use of a magnetic field. Remote control drug release from the nanodevice in a cancerous cell line (HeLa) was successfully accomplished using the same induction scenario. When nanodevices equipped with quantum dots are taken into cancerous cells, they are able to provide real-time drug dose information through a corresponding variation in emission spectrum. The nanodevice designed in this study has achieved its potential as a cell-based drug-delivery system for therapeutic applications.

1. Introduction

Surface modification with functional attachments is a widely used technical strategy to enhance biological, optical, and chemical functionality of materials in a wide variety of biomedical applications, such as imaging, diagnosis, drug delivery, implants, and so on.[1–10] Recently, the development of multifunctional, nanomedical platforms, through a skillful combination of different nanostructured materials, has been proposed. Owing to the specific advantages of these nanomaterials, many studies have been done on multimodal imaging and simultaneous therapy.[11–19] For example, magnetic nanoparticles were infused with a fluorescent dye to construct multimodal imaging probes.[17,18] Among the many nanoparticulate systems, semiconductor nanocrystals, known as quantum dots (QDs), confer advantages over traditional fluorescent molecules, such as organic dyes. This is because of their unique optical properties, including narrow photoluminescence (PL) spectra, low photoleaching, and high resistance to chemical degradation.[8] QDs have also been reported to carry therapeutic agents for healing applications.[12] The combination of both imaging and therapeutic functions in nanoparticles introduces an attractive advance in the field of biomedicine, diagnosis, and pharmaceuticals.

Surface-modified, magnetic nanoparticles are widely used in the field of biomedicine, including drug/gene delivery,[20–23] bioseparation,[24] magnetic resonance imaging,[25–27] and hyperthermia therapy.[27] A magnetic field provides a noncontact force, allowing remote management of dosing, where the field triggers drug release from the magnetic drug carriers.[28,29] In our previous studies, we extensively characterized the magnetic-sensitive properties of a ferrogel under a high-frequency magnetic field (HFMF). Drug release from the ferrogel was effectively activated via an external magnetic field.[30] Derfus et al. demonstrated that the magnetic platform had the ability to remotely trigger release of biomolecules from its surface. This was done in vivo using radio-frequency electromagnetic field (EMF) activation, which enhances penetration depth over heat.[31] However, there has been little investigation into fast-response, controlled drug release from nanoscaled platforms under magnetic stimulation, or monitoring of the release of therapeutic molecules in a quantitative manner. Therefore, an integration of these functions will be technically significant in developing a multifunctional nanodevice capable of simultaneous imaging, controlled drug delivery, and in situ monitoring of drug release with molecular resolution.

In our earlier research, we developed a new type of magnetic core/shell nanocapsule that allows active molecules to be expelled in the presence of a remotely controlled magnetic field.[32] The release of the active molecules from the nanocapsules can be finely tuned according to exposure time in the magnetic field.

[*] Prof. D. M. Liu, Prof. S. Y. Chen, Dr. S.-H. Hu, Dr. K.-T. Kuo, Dr. W.-L. Tung
Department of Materials Sciences and Engineering
National Chiao Tung University
Hsinchu, 300 (Taiwan)
E-mail: deanmo_liu@yahoo.ca; sanyuanchen@mail.nctu.edu.tw

DOI: 10.1002/adfm.200900465

However, it would be desirable to further engineer the nanocapsules to monitor the release of active molecules at nanometric or cellular resolution. We also believe that a nanocapsule should be able to provide easily monitored, high-resolution optical information, viewable via simple spectroscopic methods, rather than conventional MRI imaging. On this basis, here, we designed a new drug-delivery nanodevice by deposition of quantum dots, namely, Zn−Cu−In−S (ZCIS) nanocrystals,[33] onto the surface of a core/shell drug-delivery nanocapsule recently developed,[32] to form a nanometric multifunctional platform. The core/shell nanocapsule consists of a polymer core covered with a thin layer of single-crystal iron oxide shell. This unique core/shell structure offers great therapeutic potential for controllable drug release, with dosage controlled via an external magnetic field. The quantum dots deposited on the surface of the magnetic nanoparticles are used for directly monitoring the release of the drugs. This is achieved by observing variations in the fluorescence intensity of the quantum dots. This property of the QDs varies with absorption of thermal energy, matching the excitation binding energy of QDs. Free carriers generated by exciton dissociation can tunnel between nearby QDs, causing a decrease in the fluorescence intensity.[34,35] While the QDs are attached to the surface of the magnetic nanoparticles, the heat energy induced by the external HFMF can transfer from the magnetic shell to the QDs via the magnetic nanoparticles. Since this design is conceptually and technically achievable, it is further believed that the attachment of the ZCIS QDs on the surface of the nanocapsules may act not only as a strong fluorescence-emitting agent, but also as a nanometric sensor to monitor drug release, in real-time, within a magnetic field.

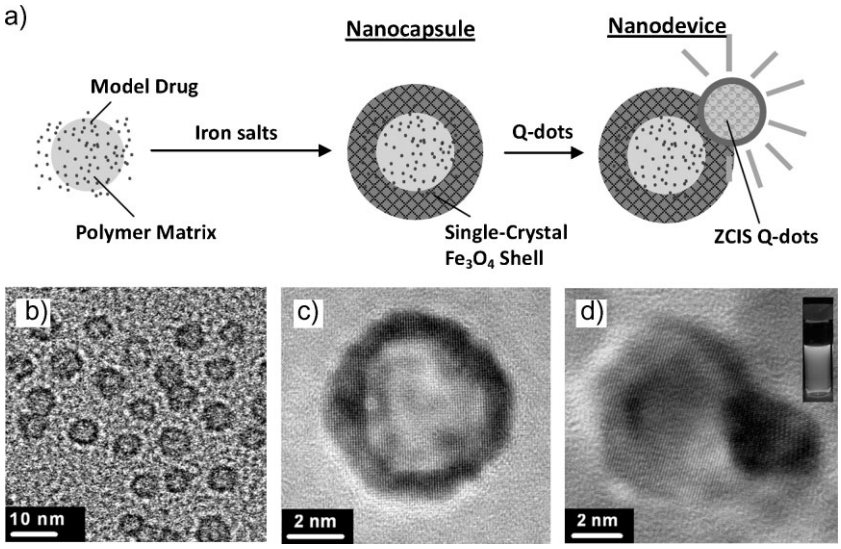

Figure 1. a) Schematic of the stimuli-response nanodevice delivery system where quantum dots were deposited on the shell of the PVP/Fe_3O_4 core/shell nanospheres. Attachment of the ZCIS QDs on the surface of the nanospheres acts not only as a strong fluorescence-emitting agent, but also as a sensor to monitor the drug release in a real-time basis under magnetic induction. b) Transmission electron microscopy (TEM) image and c) high-resolution (HR)TEM image of the PVP/Fe_3O_4 core/shell nanospheres. d) HRTEM image of the ZCIS-doped nanospheres. After incorporation of the ZCIS QDs on the core/shell nanospheres, the suspension displayed a fluorescence character under UV light (inset).

2. Results and Discussion

2.1. Preparation of a Multifunctional Nanodevice

The procedure for synthesis of magnetic nanocarriers is schematically illustrated in Figure 1a. Poly(*N*-vinyl-2-pyrrolidone) (PVP) nanoparticles, containing a test molecule such as a fluorescent dye, were prepared through a self-assembly process in benzyl ether. After self-assembly, the PVP molecules are aggregated into a micelle structure. Drug molecules are embedded within the amphiphilic nature of the PVP.[36–38] Following micelle formation, a thin layer of iron oxide is deposited on the core surface in single-crystal form. The resulting PVP/Fe_3O_4 core/shell nanocapsules, shown in Figure 1b, display a spherical geometry ranging from 10 to 15 nm in diameter. High-resolution transmission electron microscopy (HRTEM), shown in Figure 1c and in the Supporting Information (Fig. S1), confirms that the structure of the nanospheres is an amorphous core and a thin, single-crystal shell, which suggests self-organization of the iron oxide precursor upon nucleation and growth in the presence of the PVP. Although limited to metallic crystals, this agrees with an earlier study of a similar synthesis scenario.[39,40] In the current core/shell system, iron ions can be efficiently anchored onto the pyrrolidone ring of PVP. This provides epitaxial-like growth of the oxide to form a single-crystal structure. After the core/shell nanocapsules were synthesized, ZCIS quantum dots were prepared and grown on the shell surface. A procedure described by Nakamura et al. is used to form Fe_3O_4 shell–ZCIS heterodimers.[41] A HRTEM image, shown in Figure 1d, shows the solid particle residing on the ring-like shell, corresponding to a ZCIS heterodimer. Energy dispersive X-ray spectrometry (EDS) analysis confirms that the ring-like region mainly consists of Fe and the small solid particle consists of Cu and S, shown in the Supporting Information (Fig. S2). The local Fourier transfer pattern also demonstrates a high crystallinity of the ZCIS QD. After incorporation of the ZCIS QDs onto the shells, the resulting suspension shows a strong yellow appearance under UV exposure. This can be seen in the inset picture of Figure 1d and suggests that these ZCIS-modified nanocapsules (hereafter called nanodevices) can be used not only as drug nanocarriers but also as nanoprobes for imaging (see Supporting Information, Fig. S3). The magnetic properties of the nanodevices and nanocapsules were measured by SQUID (superconducting quantum interference device) at 298 K, with the magnetic field sweeping from −10 000 to +10 000 G. The correlation of magnetization with magnetic field for both the nanodevices and the nanocapsules, shown in Figure 2, demonstrates a similar shape with negligible hysteresis, showing superparamagnetic behavior. The saturation magnetization (M_s) of the nanodevices is smaller than that of the nanocapsules because of the dilution effect.

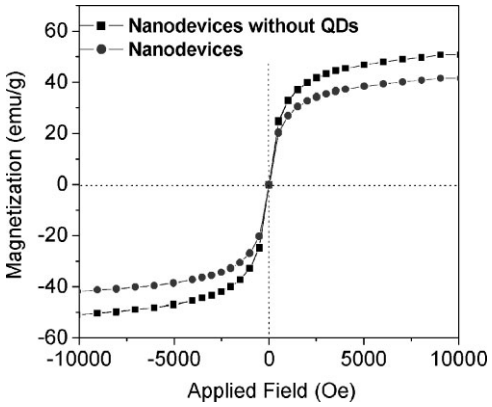

Figure 2. Field-dependent magnetization curve of nanodevices with and without quantum dots.

2.2. Drug Release and In Situ Monitoring Abilities of the Nanodevices

The nanodevices were surface-modified and conjugated with a targeting ligand, folic acid (FA), to cause hydrophilic behavior. The process is illustrated in the Supporting Information, Figure S4. After modification of the nanodevices, a stable aqueous suspension was prepared. The fluorescence spectrum of the ZCIS remained identical to the initial preparation, indicating that folic acid imparts no adverse effect on the optical properties of the ZCIS QDs. The suspension was subjected to a high-frequency magnetic field for investigation of the drug release mechanism. Prior to magnetic stimulation, the green-fluorescence loaded nanocapsules showed no sign of release in 24 h of storage in an ambient environment. This was confirmed via photoluminescence (PL) spectroscopic monitoring and suggests that the dye molecules are encapsulated in the core phase for a long period of time without any unwanted leakage. However, subjection to the HFMF for varying lengths of time, as shown in Figure 3a, reveals an interesting phenomenon (see Supporting Information, Fig. S5). The intensity of the dye emission peak at 517 nm increased with the duration of the magnetic field. In contrast, the intensity of the emission peak from the ZCIS QDs showed an inverse relationship, a decrease in emission intensity. The increase in peak intensity with time upon magnetic stimulation indicates a magnetically induced release of dye molecules from the nanodevices. In a recent study, such a release can be easily and precisely controlled with manipulation of the surrounding magnetic field; from a burst-like profile upon stimulation to a zero-release profile immediately after removal of the magnetic field.[32] The emission peak from the ZCIS quantum dots showed strong PL intensity at the beginning of the stimulus. However, as time elapsed, a gradual reduction in peak intensity together with a red-shift of the PL spectra for the QDs was clearly detected over an operation time of 100 s. The peaks for the dye and QDs reacted oppositely under the same magnetic stimulus, implying a potential correlation of both spectra.

Bias may arise when determining whether the correlation is simply coincidence or a rule in this nanosystem. To avoid this, magnetic fields of varying intensities were applied. This aimed to determine whether the correlation of the spectra between drug release and quantum-dot emission is sustainable over a range of

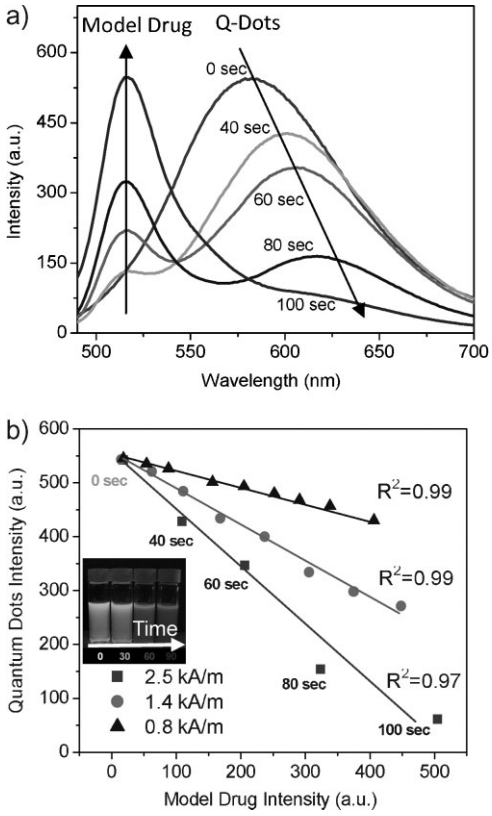

Figure 3. a) Emission spectra of dye-loaded nanodevices (30 mg per 10 mL water) under HFMF treatment over a time period of 0 to 100 s. Before HFMF exposure, the dye-loaded nanodevices displayed no sign of dye release, which causes green fluorescence at an emission wavelength of 517 nm, as determined by fluorescence spectrophotometry. However, a strong emission signal from the QDs after exposure, red fluorescence at an emission wavelength of 581–614 nm, shows that dye was released from the nanodevices. A degenerative green florescence appeared concurrently. b) Model drug intensity versus QD intensity curves originate from both the dye and ZCIS emitting spectra and show a near symmetrical profile under different magnetic-field strengths. This strongly indicates that dye release can be precisely monitored and quantitatively estimated along with the spectral variation of the ZCIS QDs from the nanodevices.

operating intensities, from 0.8 to 2.5 $kA\,m^{-1}$ in the current magnetic system. The resulting correlation in the magnetically induced changes of the spectra are given in Figure 3b. A linear relationship exists between the spectral intensity of dye molecules and the QD emission. The correlation coefficient over a range of the data reaches 0.97–0.99 and can be obtained for different magnetic intensities. The quantity of drug released relied mainly on the strength of the magnetic field under short-term induction. This implies that a weaker magnetic field results in the slower release of drugs. A linear relationship exists over the entire range of operating conditions. Although the emission spectra were measured from two independent sources, this finding strongly suggests that the drug release from the nanodevice can be quantitatively correlated with in vitro, doped ZCIS QDs to a high precision. Dye release can be precisely monitored along with the spectral variation of the ZCIS QDs from the nanodevices. This finding is in agreement with the hypothesis that two independent

mechanisms can be triggered simultaneously from a given magnetic field, and that the mechanisms will also be quantitatively correlated. We believe that this highly correlated relationship may also be adopted for in situ monitoring of cellular systems. This will be explained further.

2.3. Spectral Variation of the ZCIS QD Under Magnetic Induction

The mechanism causing the spectral variation of the ZCIS QDs upon magnetic induction is of great interest. To further explore the possible causes, a separate photoluminescence test for the ZCIS QDs was performed in the same magnetic field; no detectable sign of change in the emitted spectrum was observed. This indicates an invariance in the spectral properties of the ZCIS QDs with respect to magnetic field. Since the variation of emitted spectrum for quantum dots has been proven to be associated with a change in the band energy structure or surface composition of the QDs, it is highly plausible that a number of factors cause changes in the resulting spectrum of the ZCIS QDs. These changes may include magnetically induced heating, surface adsorption of the dye molecules, and/or surface corrosion caused by the presence of water. However, according to experimental observation, the above factors have to be rapidly responsive and probably interdependent since the decrease in the emission intensity and a red-shift of the spectra occurred relatively quickly, in less than 20 s, in the presence of the magnetic stimulation at 2.5 kA m^{-1}. More interestingly, it is evident that the spectral variation has experimentally proven to be irreversible. These observations suggest that a permanent change in either chemical or physical structure has been induced rapidly on the ZCIS QDs while the nanodevices were subjected to the magnetic stimulus.

To further explain the reasons behind the spectral degeneration of the QDs under short-term induction, nanodevices not carrying the dye molecules were prepared and exposed to the same magnetic field. The resulting emission spectra were identical to the case of the nanodevices with the dye. This indicates that dye molecules exerted little or no influence on the resulting PL emission spectra of the ZCIS QDs. The PL spectrum of the dye molecules remained identical in shape and emission peak position to that given in Figure 2, suggesting that the dye molecules, after release into an aqueous environment, remained chemically and physically stable. There is a magnetically induced temperature rise, or hot spot, on the shell of the nanodevice due to magnetic energy dissipation from single-domain particles, such as a Brown and/or Neel relaxation; this has been verified in a number of recent studies.[42] From experimental observation, the temperature of the solution that contained the nanodevices gradually rises. As shown in Figure 4, while applying a high-strength magnetic field of 2.5 kA m^{-1}, the temperature of the solution increased to about 40 °C in 4 min. Since the temperature rise of the solution is solely resulting from the energy dissipated from the magnetic nanodevices, the temperature of the nanodevice itself should be much higher and can be calculated by the thermodynamic relationship: $\Delta H = m_w C_w \Delta T_w = m_m C_m \Delta T_m$, where C_w and C_m are the specific heat capacity of water and the magnetic material, respectively, m is the mass of the component, and T and H are the temperature and enthalpy, respectively. Neglecting any heat loss to the surrounding water, the temperature of the nanodevices, after subjection to the HFMF for 1 min, can raise to approximately 200 °C in a field strength of 2.5 kA m^{-1}. Heat transfer from the shell to adjacent QDs occurs rapidly, causing quick equilibration with the water environment. However, once the QDs were heated, free carriers of exciton dislocations in QDs tunnel to the surrounding environment, causing a deterioration of the emitted fluorescence intensity.[34] Therefore, the temperature rise of the QDs may cause a certain degree of thermal corrosion, such as surface oxidation or thermally induced structural variation of the ZCIS QDs. This would permanently change the surface structure of the ZCIS QD. This change has been confirmed by X-ray photoelectron spectroscopy (XPS), as shown in Figure 5. A change in the binding energy spectrum of the S 2p peak of the ZCIS

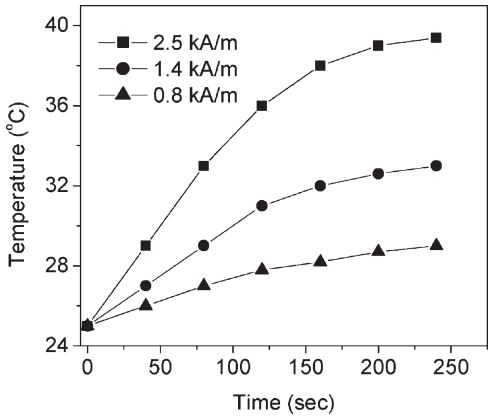

Figure 4. Temperature curve of nanodevices during application of HFMFs of different strengths.

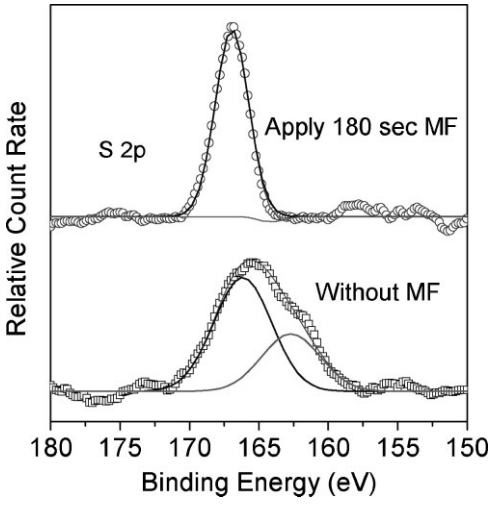

Figure 5. Binding energy of S 2p of the nanodevices with and without exposure to a HFMF for a time period of 180 s. XPS results indicate the binding energy shift of the S 2p line from 162.3 to 166.2 eV, before the stimulus, to a single, strong binding-energy peak at 167 eV, after the magnetic exposure. This could be attributed to S^{2-} from ZnS, CuS, In_2S_3, or SO_4^{2-}, SO_2. The binding energy at 167 eV on the ZCIS surface is strongly associated with the presence of oxide groups, including SO_4^{2-} and SO_2, on the surface. This demonstrates rapid oxidation of the ZCIS QDs after a short period of magnetic induction.

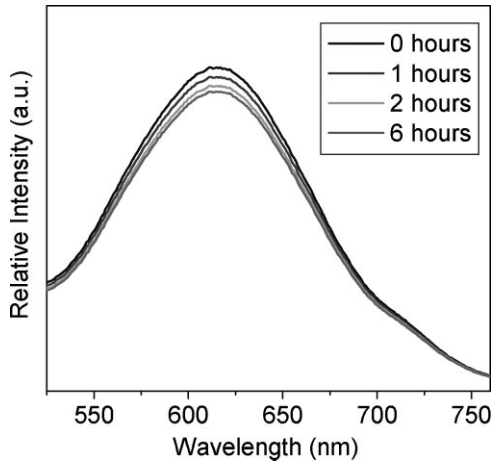

Figure 6. PL emission spectra at various time intervals of nanodevice incubation in PBS solution.

QDs, from 162.3 eV before the stimulus to 167 eV after the stimulus, is clearly detected. For the latter, the binding energy is associated with the presence of oxide groups such as SO_4^{2-} or SO_2, which strongly suggests a rapid oxidation occurred on the ZCIS surface under short-term magnetic induction. The associated, thermally induced emission deterioration of both mechanisms mentioned above explains the degeneration of emission behavior and spectral-shift of the ZCIS QDs upon magnetic stimulation. However, it is difficult to clearly differentiate the degenerative contribution in a quantitative manner from either mechanism. We simply consider the degeneration of both as a single event for the following discussion.

An important concern for practical applications of this nanodevice is whether the emission degeneration of the attached QDs occurs spontaneously without the presence of the magnetic field over a reasonable time period in a physiological environment. If spontaneous degeneration occurs, the correlation depicted in Figure 3 becomes unreliable. To examine this possibility, a simple test was performed by incubating the nanodevices in phosphate buffered saline (PBS) solution for a time period of 6 h, followed by measuring the PL emission spectrum at various time intervals, as shown in Figure 6. Fortunately, the resulting PL spectra of the QDs remained identical over the evaluation time span. This confirms the reliability of the linear relationship given in Figure 3 and further substantiates the correlation between two optical spectra as sustainable in vitro. However, it is more technically important from the current research that both spectral variations, the one from the dye spectrum and the PL emission of the ZCIS, are able to work independently but are well-correlated. In other words, the attached ZCIS QD can act as a nanometric sensor to monitor the quantity of drug released from the drug-carrying nanodevice. This multifunctional assembly, imaging, drug delivery controller, and in situ monitor, when integrated onto the nanodevice, may enable new pathways to advance nanotherapeutic technology.

2.4. Operation Mechanism of the Nanodevice

Based on the mechanism of degeneration of the emission spectrum of the ZCIS QDs and the deformation mechanism of the

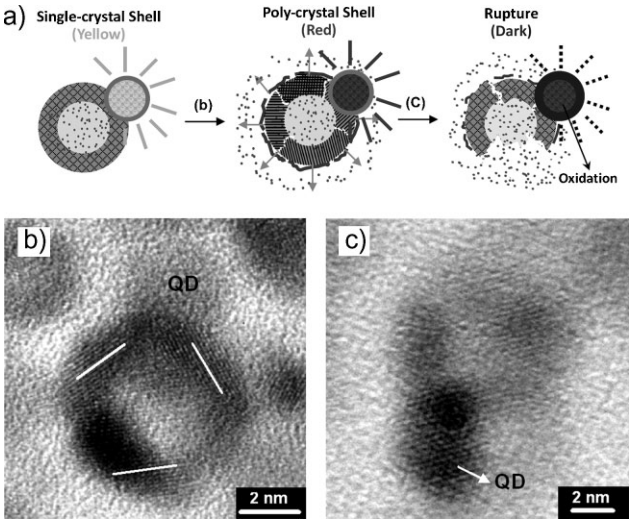

Figure 7. a) Schematic illustration of the nanodevice with a proposed mechanism for controlled release of the dye molecules, as well as the degeneration of fluorescence intensity of the ZCIS QDs. b) Shell vibration causing enlargement of the dimensions of nanocrevices along the deformed single-crystal shell, rendering dye release upon short-term magnetic stimulation. c) After long-term exposure, the deformed shell has received a sufficient amount of the energy to cause a final, permanent, mechanical rupture. Meanwhile, rapid surface oxidation altered the surface structure of the QDs, leading to substantial degeneration of the fluorescence intensity.

shell, outlined in a previous investigation,[32] we propose an operation mechanism for the nanodevice in a magnetic field. Figure 7a shows a schematic drawing of the mechanism of drug release and shell deformation associated with the structural degeneration of the attached QDs. Accordingly, after 60 s of exposure to the stimulus, the single-crystal nanoshell structure was subjected to lattice deformation, forming nanometer-sized polycrystals of varying orientations, shown in Figure 7b. Nanometric scale boundaries between the nano-polycrystalline domains formed and provided numerous nanoconduits that allow leaking of the dye molecules to the environment. In other words, for short-term induction, extremely small cracks or crevices were formed along the boundary regions of the thin iron oxide shell and are kept open by the presence of the magnetic field. Extended magnetic stimulus enlarged the nanocrevices until permanent rupturing of the shell occurred. At this time, the dye molecules were released from the nanodevice easily and completely, as shown in Figure 7c. Meanwhile, the energy structure of the ZCIS QDs altered considerably as a result of thermally induced photoleaching along with surface oxidation. This resulted in degeneration of the fluorescence intensity. While the shell was undergoing permanent rupture, the bandgap structure of the QDs was irreversibly altered, turning a dark red after about 100 s at a magnetic field strength of 2.5 kA m^{-1}.

2.5. In Situ Monitoring of Drug Release in Cancerous Cells

To understand the optical behavior of the nanodevices within cells, they were modified using mercaptoundecanoic acid (MUA)

followed by crosslinking with lysine to form a hydrophilic layer that exhibits both carboxyl and amine groups on its surface.[43] Folic acid (FA) molecules were attached to the functional layer on the surface using carbodiimide chemistry to form bioconjugates. Folate receptors (FR) act as cancer-cell-targeting ligands due to overexpression in many human cancerous cells, including mammary gland, lung, kidney, colon, prostate, and throat cells. However, they are only minimally distributed in normal cells.[44] Folic acid exhibits high affinity to FR and is expected to allow the nanodevice to efficiently attach on or enter into cancerous cells via receptor mediated endocytosis. Incubation of the HeLa (human cervical cancer cells) cell line with the MUA-modified nanodevices (MUA-NDs) and FA-modified NDs (FA-NDs) were completed separately. Both the MUA-NDs and FA-NDs were incubated with the cells for a period of 4 h. The majority of the FA-NDs can be clearly observed in the cytoplasm region of the cell, but only a few of the MUA-NDs were attached or taken by HeLa cells, indicating that the FA-modified version promotes cellular uptake, as shown in the Supporting Information, Figure S5. It is expected that higher attachment or cellular uptake due to FA modification imparts enhanced therapeutic potential for the nanodevices. Figure 8 shows the results of the MTT (3-(4,5-dimethyldiazol-2-yl)-2,5 diphenyl tetrazolium bromide) assay, as a measure of metabolic competence of the cell with FA-NDs of different concentrations. The difference in the cytotoxicity over an incubation period of 12 to 48 h is negligibly small. At the highest concentration of 1 $\mu L\,cm^{-3}$ FA-NDs, the cell viability remained at approximately 96%. The results suggest that the nanodevices show minimal toxicity for the HeLa cells. After cellular uptake, controlled drug release and real-time, in situ monitoring of the ZCIS QDs were performed in a magnetic field with a strength of 2.5 $kA\,m^{-1}$. As illustrated in Figure 9 (Supporting Information, Fig. S6), an increase in the duration of the field from 0 to 180 s caused the dye molecules (green channel) to be released rapidly within the cells, while the corresponding fluorescence intensity of the ZCIS QDs (red channel) decreased. Digital software (Nikon, Japan) was used to analyze the fluorescence intensities of both the dye molecules and ZCIS QDs. B_{sum}, G_{sum}, and R_{sum} represent the total intensity of the blue, the green, and the red channels in the images, respectively.

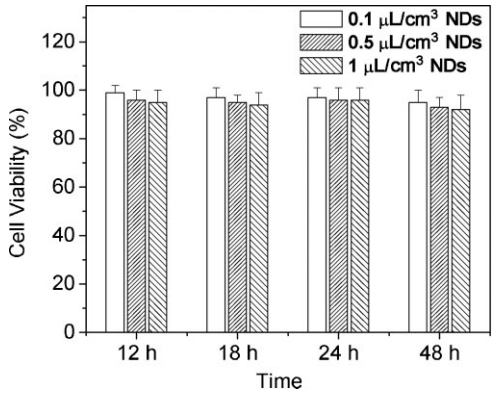

Figure 8. Cell viability of HeLa cells after 12 to 48 h of incubation with increasing amounts of FA-modified nanodevices (FA-NDs). Cell viability was measured using an MTT assay.

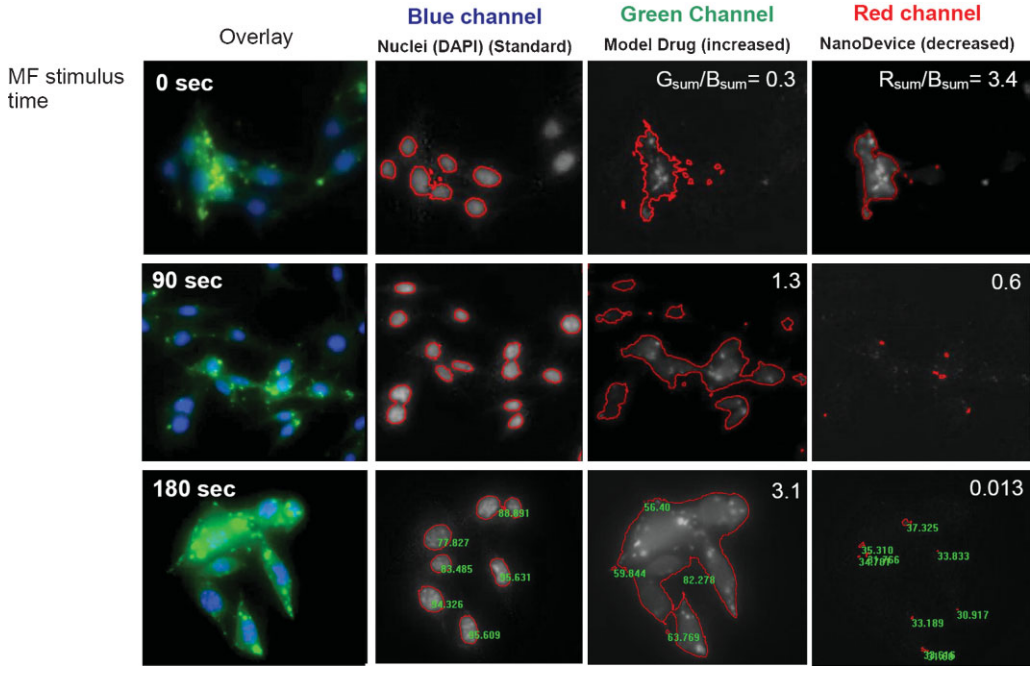

Figure 9. Fluorescent combination of the HeLa cells with the dye-loaded nanodevices after 12 h incubation. With increasing duration of HFMF treatment, both the controlled release of the dye molecules (green channel intensity increased) and the associated real-time, in situ monitoring capability of the doped ZCIS QDs (red channel intensity decreased) can be manipulated simultaneously to single-cell resolution. This implies that dye release can be precisely monitored by the variation of the ZCIS QDs from the nanodevices. G_{sum}/B_{sum} represents the intensity ratio of the green to blue channels, and is indicative of the relative concentration of the model drug in each cell. R_{sum}/B_{sum} is then defined as the relative intensities of the nanodevices in each cell.

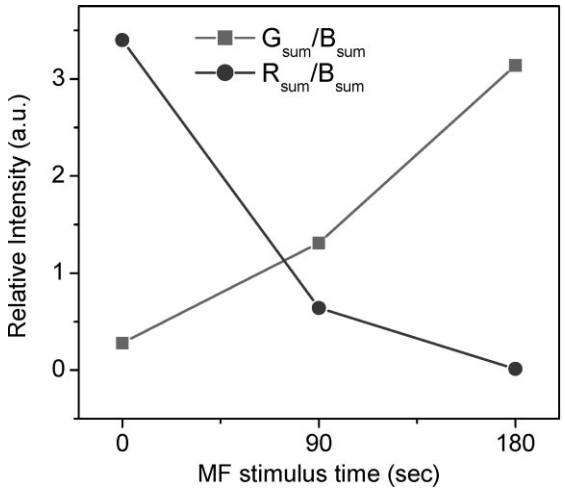

Figure 10. The ratios of G_{sum}/B_{sum} and R_{sum}/B_{sum} versus the duration of magnetic stimulus in the cells gives rise to two curves. The results demonstrate the relative drug concentration, represented by G_{sum}/B_{sum}, in the cells with increasing duration of stimulus. The fluorescence intensity originating from the ZCIS QDS, represented by R_{sum}/B_{sum}, decreased in proportion at the same time.

The blue fluorescence was due to the 4′,6-diamidino-2-phenylindole(DAPI)-dyed nuclei and was expected to be relatively similar for each cell. Therefore, the intensity of the blue channel was assumed to be standard for each image. G_{sum} and R_{sum} are from drug release and quantum dots, respectively. G_{sum}/B_{sum}, the ratio of the green channel intensity to the blue channel intensity, is indicative of the relative concentration of the dye molecules in each cell. Similarly, R_{sum}/B_{sum} is the value of the relative intensities of the nanodevices in each cell. After measurement, statistical analysis of fluorescence intensities exhibited a strong correlation between dye release and spectral variation of the ZCIS within the cells, as shown in Figure 10. The ratios of G_{sum}/B_{sum} and R_{sum}/B_{sum} versus duration of the magnetic field in the cells gives rise to two separate curves. These curves show that the relative drug concentration, represented by G_{sum}/B_{sum}, in the cells increases with the duration of stimulus. The fluorescence intensity of the nanodevice, originating from the ZCIS QDs and represented by R_{sum}/B_{sum}, decreased in proportion at the same time. There are two purposes to the cell culture test. The first purpose is a test of the short-term cytocompatibility nature of the nanodevice, where the HeLa cells appeared to be viable over the duration of the culturing step. The second and most critical purpose is the test of the in vitro monitoring capability of the nanodevices, where drug dosage can be quantitatively traced within a single cell.

3. Conclusion

The multifunctional drug-delivery nanodevice makes use of quantum dots to successfully image, target, and deliver drugs via remote control. The devices also have the capability to monitor the in situ drug release within a model cancerous cell line, HeLa cells, to cellular resolution. These nanodevices offer outstanding control of release and retention for the molecules encapsulated inside their polymer core. The dense, single-crystalline shell prevents the fluorescent dye from escaping prior to the desired release. Furthermore, the nanodevices are able to monitor real-time drug dosage through corresponding variation in emission spectrum of the quantum dots within the HeLa cells. The nanodevices have great potential advantages as a cell-specific drug-delivery system for therapeutic applications. With the in situ monitoring capability of the nanodevice, we believe that both target-oriented therapy and diagnosis can be integrated and managed within a single cell. Multifunctional nanometer-scaled platforms are expected to open a new avenue in the development of multifunctional therapeutic nanosystems. An in vivo analysis is currently underway to treat brain tumors in mice.

4. Experimental

Preparation of the Nanodevices: Synthesis of the PVP/Fe_3O_4 core/shell nanospheres was reported in our previous work [35]. To encapsulate the model drug, fluorescent molecules, in the polymer matrix, 4 wt% polyvinylpyrrolidone (PVP; weight-average molecular weight, Mw, ~10 000; Sigma) was dissolved in D.I. (deionized) water and preheated to 80 °C. Then fluorescent molecules were added into the solution and mixed for 6 h. In suitable concentrations, the PVP molecules will assembly themselves as nanospheres in the solution, forming drug-loaded PVP nanoparticles. Under a nitrogen atmosphere, $FeCl_3 \cdot 6H_2O$ and $FeCl_2 \cdot 4H_2O$ with a $FeCl_2/FeCl_3$ molar ratio of 2:1 were dissolved into water and mixed with the drug-loaded PVP nanoparticles under vigorous stirring at 80 °C. After 4 h, the iron salts were deposited on the surface of the drug-loaded PVP nanoparticles. This was achieved via slow addition of 2 mL of ammonium water (NH_4OH, 33%), causing precipitation so that iron oxide shells were immediately formed on the PVP nanoparticle surfaces. At this stage, a drug-loaded PVP/iron oxide core/shell nanosphere exists in the solution. Precipitated powders were collected by centrifugation at 6000 rpm, removed from the solution, and washed in D.I. water four times. The PVP/Fe_3O_4 core/shell nanospheres were separated by the centrifugation. The average diameter of the core/shell nanospheres was about 12–20 nm.

To grow the ZCIS quantum dots on the surface of the PVP/Fe_3O_4 core/shell nanospheres, the latter were redispersed in trioctylphosphine (TOP, 90%, technical grade) with diethyldithiocarbamic acid zinc salt, $[(C_2H_5)_2NCSS]_2Zn$. The solution was diluted with octadecene (ODE, 90%, technical grade) to form Solution 1. Then, CuCl and $InCl_3$ were dissolved in oleylamine at 50 °C to form Solution 2. The two solutions were mixed and heated to 140 °C in a nitrogen atmosphere for several minutes. Deposition of quantum dots (QDs) on the surface of the PVP/Fe_3O_4 core/shell nanospheres caused the solution to turn yellow.

Characterization: The formation of nanostructures was investigated using transmission electron microscopy (JEM-2010, Japan). A high frequency magnetic field (HFMF) at 50–100 kHz was applied to the magnetic nanodevices to investigate their drug release behavior. The HFMF was created using a power supply, a functional generator, an amplifier, and coolant water. Similar equipment was reported in the literature [45]. The strength of the magnetic field depends on the coils. In this study, the coils consisted of eight loops. The frequency was 50 kHz and the magnetic field strength (H) was 2.5 kA m^{-1}. The temperature of the HFMF generator was controlled by cycling water at 25 °C. The drug release behavior from 0.05 wt% magnetic nanodevices was measured in 20 mL of phosphate buffered saline (pH 7.4). PL spectroscopy (fluorescence spectrophotometer F-4500, Hitachi, Japan) was used to characterize the release profile of the dye molecules and the fluorescence intensity of nanodevices after application of a HFMF of 50 kHz. The nanodevices, at a concentration of 0.05 wt%, were dispersed in the water solution for varying durations. X-ray photoelectron spectroscopy (XPS) was performed in an ESCALAB 250 instrument (Thermo VG Scientific, West Sussex, UK),

equipped with a Mg Kα source at 1253.6 eV at the anode. The chemical shifts of the XPS peaks were standardized with respect to the C 1s peak at 284.6 eV.

Cell Culture and In Situ Monitoring of Drug Release: HeLa, human cervical cancer cells, were maintained in Dulbecco's modified Eagle's medium (DMEM) with 10% fetal bovine serum, 100 units mL^{-1} penicillin, and 100 $\mu g\,mL^{-1}$ streptomycin. Cells were cultured at 37 °C in a humidified atmosphere of 5% CO_2 in air. The nanodevices were incubated with the cells for 12 h. The cells were then subjected to a HFMF for 0, 90, and 180 s. Results were observed by PL microscopy (Nikon TE-2000U, Japan). Digital analysis software (Nikon, Japan) was used to analyze the fluorescence intensities of the model drug and the nanodevices. The conditions of exposure were the same for each color channel. Analysis was done by Nikon C1 software, which defined the fluorescence intensity from 1 to 255. The ranges of the fluorescence intensities were: blue channel (60–255), green channel (40–255), and red channel (30–255).

Acknowledgements

This work was financially supported by the National Science Council of the Republic of China, Taiwan, under contracts NSC-2113-M-009-027-MY2, NSC-97-2627-B-009-002, and, NSC 98-2113-M-009-004. Supporting Information is available online from Wiley InterScience or from the author.

Received: March 18, 2009
Published online: October 6, 2009

[1] B. J. Nehilla, P. G. Allen, T. A. Desai, *ACS Nano* **2008**, *2*, 538.
[2] R. Haag, F. Kratz, *Angew. Chem. Int. Ed.* **2006**, *45*, 1198.
[3] M. Liong, J. Lu, M. Kovochich, T. Xia, S. G. Ruehm, A. E. Nel, F. Tamanoi, J. I. Zink, *ACS Nano* **2008**, *2*, 889.
[4] X. Gao, Y. Cui, R. M. Levenson, L. W. K. Chung, S. Nie, *Nat. Biotechnol.* **2004**, *22*, 969.
[5] J. H. Lee, J. H. Lee, Y. M. Huh, Y. W. Jun, J. W. Seo, J. T. Jang, H. T. Song, S. Kim, E. J. Cho, H. G. Yoon, J. S. Suh, J. Cheon, *Nat. Med.* **2007**, *13*, 95.
[6] K. T. Yong, I. Roy, H. E. Pudavar, E. J. Bergey, K. M. Tramposch, M. T. Swihart, P. N. Prasad, *Adv. Mater.* **2008**, *20*, 1412.
[7] L. Brannon-Peppas, J. O. Blanchette, *Adv. Drug Delivery Rev.* **2004**, *56*, 1649.
[8] I. L. Medintz, H. T. Uyeda, E. R. Goldman, H. Mattoussi, *Nat. Mater.* **2005**, *4*, 435.
[9] I. F. Li, C. H. Su, H. S. Sheu, H. C. Chiu, Y. W. Lo, W. T. Lin, J. H. Chen, C. S. Yeh, *Adv. Funct. Mater.* **2008**, *18*, 766.
[10] C. Sun, O. Veiseh, J. Gunn, C. Fang, S. Hansen, D. Lee, R. Sze, R. G. Ellenbogen, J. Olson, M. Zhang, *Small* **2008**, *4*, 372.
[11] S. Santra, R. P. Bagwe, D. Dutta, J. T. Stanley, G. A. Walter, W. Tan, B. M. Moudgil, R. A. Mericle, *Adv. Mater.* **2005**, *17*, 2165.
[12] L. Qi, X. Gao, *ACS Nano* **2008**, *2*, 1403.
[13] J. Kim, S. Park, J. E. Lee, S. M. Jin, J. H. Lee, I. S. Lee, I. Yang, J. S. Kim, S. K. Kim, M. H. Cho, T. Hyeon, *Angew. Chem. Int. Ed.* **2006**, *45*, 7754.
[14] J. Dobson, *Nat. Nanotechnol.* **2008**, *3*, 139.
[15] E. Tasciotti, X. Liu, R. Bhavane, K. Plant, A. D. Leonard, B. K. Price, M. M. C. Cheng, P. Decuzzi, J. M. Tour, F. Robertson, M. Ferrari, *Nat. Nanotechnol.* **2008**, *3*, 151.
[16] J. H. Lee, Y. W. Jun, S. I. Yeon, J. S. Shin, J. Cheon, *Angew. Chem. Int. Ed.* **2006**, *45*, 8160.
[17] W. J. M. Mulder, R. Koole, R. J. Brandwijk, G. Storm, P. T. K. Chin, G. J. Strijkers, C. de M. Donegá, K. Nicolay, A. W. Griffioen, *Nano Lett.* **2006**, *6*, 1.
[18] C. P. Tsai, Y. Hung, Y. H. Chou, D. M. Huang, J. K. Hsiao, C. Chang, Y. C. Chen, C. Y. Mou, *Small* **2008**, *4*, 186.
[19] X. Michalet, F. F. Pinaud, L. A. Bentolila, J. M. Tsay, S. Doose, J. J. Li, G. Sundaresan, A. M. Wu, S. S. Gambhir, S. Weiss, *Science* **2005**, *307*, 538.
[20] S. H. Hu, D. M. Liu, W. L. Tung, C. F. Liao, S. Y. Chen, *Adv. Funct. Mater.* **2008**, *18*, 2946.
[21] T. J. Yoon, J. S. Kim, B. G. Kim, K. N. Yu, M. H. Cho, J. K. Lee, *Angew. Chem. Int. Ed.* **2005**, *44*, 1068.
[22] R. J. Mannix, S. Kumar, F. Cassiola, M. Montoya-Zavala, E. Feinstein, M. Prentiss, D. E. Ingber, *Nat. Nanotechnol.* **2008**, *3*, 36.
[23] I. Koh, X. Wang, B. Varughese, L. Isaacs, S. H. Ehrman, D. S. English, *J. Phys. Chem. B* **2006**, *110*, 1553.
[24] O. Veiseh, C. Sun, J. Gunn, N. Kohler, P. Gabikian, D. Lee, N. Bhattarai, R. Ellenbogen, R. Sze, A. Hallahan, J. Olson, M. Zhang, *Nano Lett.* **2006**, *5*, 1003.
[25] C. W. Lu, Y. Hung, J. K. Hsiao, M. Yao, T. H. Chung, Y. S. Lin, S. H. Wu, S. C. Hsu, H. M. Liu, C. Y. Mou, C. S. Yang, D. M. Huang, Y. C. Chen, *Nano Lett.* **2007**, *7*, 149.
[26] W. S. Seo, J. H. Lee, X. Sun, Y. Suzuki, D. Mann, Z. Liu, M. Terashima, P. C. Yang, M. V. McConnell, D. G. Nishimura, H. Dai, *Nat. Mater.* **2006**, *5*, 971.
[27] A. Jordan, R. Scholz, P. Wust, H. Schirra, T. Schiestel, H. Schmidt, R. Felixet, *J. Magn. Magn. Mater.* **1999**, *194*, 185.
[28] Z. Lu, M. D. Prouty, Z. Guo, V. O. Golub, C. S. S. R. Kumar, Y. M. Lvov, *Langmuir* **2005**, *21*, 2042.
[29] J. Kost, R. Noecker, E. Kunica, R. Langer, *J. Biomed. Mater. Res.* **1985**, *19*, 935.
[30] S. H. Hu, T. Y. Liu, D. M. Liu, S. Y. Chen, *Macromolecules* **2007**, *40*, 6786.
[31] A. M. Derfus, G. von Maltzahn, T. J. Harris, T. Duza, K. S. Vecchio, E. Ruoslahti, S. N. Bhatia, *Adv. Mater.* **2007**, *19*, 3932.
[32] S. H. Hu, S. Y. Chen, D. M. Liu, C. S. Hsiao, *Adv. Mater.* **2008**, *20*, 2690.
[33] N. Toshima, M. Kanemaru, Y. Shiraishi, Y. Koga, *J. Phys. Chem. B* **2005**, *109*, 16 326.
[34] K. Sato,1 S. Kojima,1 S. Hattori, T. Chiba, K. Ueda-Sarson, T. Torimoto, Y. Tachibana, S. Kuwabata, *Nanotechnology* **2007**, *18*, 465 702.
[35] P. J. Carrington, V. A. Solov'ev, Q. Zhuang, A. Krier, S. V. Ivanov, *Appl. Phys. Lett.* **2008**, *93*, 091 101.
[36] X. Ye, Y. Zhou, J. Chen, Y. Sun, *Appl. Surf. Sci.* **2007**, *253*, 6264.
[37] L. Y. Hao, C. L. Zhu, W. Q. Jiang, C. N. Chen, Y. Hu, Z. Y. Chen, *J. Mater. Chem.* **2004**, *14*, 2929.
[38] M. Tsuji, N. Miyamae, S. Lim, K. Kimura, X. Zhang, S. Hikino, M. Nishio, *Cryst. Growth Des.* **2006**, *6*, 1801.
[39] Y. J. Zhu, W. W. Wang, R. J. Qi, X. L. Hu, *Angew. Chem. Int. Ed.* **2004**, *43*, 1410.
[40] Y. Sun, B. Mayers, T. Herricks, Y. Xia, *Nano Lett.* **2003**, *3*, 955.
[41] H. Nakamura, W. Kato, M. Uehara, K. Nose, T. Omata, S. Otsuka-Yao-Matsuo, M. Miyazaki, H. Maeda, *Chem. Mater.* **2006**, *18*, 3330.
[42] J. P. Fortin, C. Wilhelm, J. Servais, C. Ménager, J. C. Bacri, F. Gazeauet, *J. Am. Chem. Soc.* **2007**, *129*, 2628.
[43] W. Jiang, S. Mardyani, H. Fischer, W. C. W. Chan, *Chem. Mater.* **2006**, *18*, 872.
[44] P. S. Low, W. A. Henne, D. D. Doorneweerd, *Acc. Chem. Res.* **2008**, *41*, 120.
[45] R. Mohr, K. Kratz, T. Weigel, M. Lucka-Gabor, M. Moneke, A. Lendlein, *Proc. Natl. Acad. Sci. USA* **2006**, *103*, 3540.